Applied Materials Today 32 (2023) 101838

Contents lists available at ScienceDirect

Applied Materials Today

journal homepage: www.elsevier.com/locate/apmt

Light-induced strain and its correlation with the optical absorption at charged domain walls in polycrystalline ferroelectrics

Fernando Rubio-Marcos [a,*], Paula Pamies [b], Adolfo Del Campo [a], Jordi Tiana [c], Jonathan Ordoñez-Pimentel [b,d], Michel Venet [d], Rocío E. Rojas-Hernandez [e], Diego A. Ochoa [b], José F. Fernández [a], José E. García [b,*]

[a] Department of Electroceramics, Instituto de Cerámica y Vidrio - CSIC, Madrid 28049, Spain
[b] Department of Physics, Universitat Politècnica de Catalunya, Barcelona 08034, Spain
[c] Department of Applied Physics, Universitat de Barcelona, Barcelona 08028, Spain
[d] Department of Physics, Universidade Federal de Sao Carlos, Sao Carlos 13565-905, Brazil
[e] Department of Mechanical and Industrial Engineering, Tallinn University of Technology, Tallinn 19180, Estonia

ARTICLE INFO

Keywords:
Photoferroelectrics
Ferroelectric domain walls
Optical absorption
Barium titanate
Photoinduced strain

ABSTRACT

Photostrictive materials have a growing interest because of their great potential as light-driven actuators, among other optomechanical applications. In this context, the optical control of macroscopic strain in ferroelectrics has recently attracted remarkable attention as an effective alternative to the conventional electric control of strain. Here, a clear correlation between optical absorption and light-induced strain in polycrystalline $BaTiO_3$ is shown. Specifically, the grain size and the sample thickness dependence of optical absorption when the material is irradiated with energy photons lower than the band gap evidence that light absorption at charged domain walls is the core of the observed photo-response in ferroelectrics. The photoinduced electronic reconstruction phenomenon is proposed as the primary physical mechanism for light absorption at charged domain walls. Results open a new pathway to designing ferroelectric-based devices with new functionalities like thickness gradient-based photo-controlled nanoactuators.

1. Introduction

Photostrictive materials own the fascinating ability to convert light into mechanical strain, thereby exhibiting enormous potential to be used as active components in a new generation of nano-optomechanical systems [1–3]. Actually, the photostrictive effect has been known for more than half a century, but it has been gaining interest triggered by the progress of device miniaturization, as well as the development of sensing techniques at the nanoscale [4,5]. Nowadays, photostrictive devices are called to replace conventional micro-electromechanical ones since they are not restricted by complex wiring or circuitry, providing a feasible principle for the non-contact remote control of light-driven systems [6,7].

The light-induced nonthermal dimensional change of materials does not come from a unique physical phenomenon. For instance, the photostriction mechanism in ferroelectrics is generally acknowledged as converse piezoresponse induced by the photovoltage engendered by the bulk photovoltaic effect [8–10]. Ferroelectrics are especially interesting photostrictive materials because novel applications based on coupling mechanisms such as photostriction and piezoelectricity are expected; for instance, for optoelectrical dual source actuators [7]. In this context, the wide band gap of conventional ferroelectrics limits their photovoltaic effect-based photoresponse to the UV light spectrum, hindering the applications. Nevertheless, recent studies have demonstrated that moving ferroelectric domain walls with low-intensity visible light is possible, evidencing that a reversible optical control of the macroscopic polarization can be reached by light with photon energy below the material band gap [11,12]. As a consequence of the domain reconfiguration, mechanical strain can be easily photo-controlled, showing a linear dependence with the light intensity at several wavelengths [13].

The optical control of ferroelectric domains is fundamentally associated with ideal archetypes such as single crystals, which have high-cost mass production, hindering the rapid development of emerging light-controlled devices. Polycrystals, however, are technologically

* Corresponding authors.
E-mail addresses: frmarcos@icv.csic.es (F. Rubio-Marcos), jose.eduardo.garcia@upc.edu (J.E. García).

https://doi.org/10.1016/j.apmt.2023.101838
Received 11 February 2023; Received in revised form 20 April 2023; Accepted 30 April 2023
Available online 8 May 2023

more desirable since they can be easily manufactured on a large scale [14]. Recently, the optical control of macroscopic strain has been shown to be an effective alternative to the conventional electric control of strain in polycrystalline ferroelectrics [15–18]. Furthermore, experimental and theoretical approaches have evidenced that charged domain walls (CDWs) seem to be functional interfaces for the light-driven rearrangement of ferroelastic domain configuration [19–22], although a direct experimental relation between light absorption and photoresponse is yet to be proven. In this work, a direct correlation between visible light-induced strain and optical absorption in polycrystalline $BaTiO_3$ (BTO) is experimentally evidenced. The results represent a push towards designing and manufacturing high-performance photo--actuators based on ferroelectric ceramics, providing a reachable alternative to voltage-driven nanoactuators.

2. Experimental

2.1. Samples preparation

The samples were obtained from high-purity commercial BTO powder (Sigma-Aldrich). After grinding the powder in a high-energy ball milling, a homogeneous particle size of 0.35 μm was obtained. The milled powder was heat-treated to remove moisture and then was uniaxially (350 MPa) and isostatically (250 MPa) pressed to obtain the pellets. Three sintering schemes were designed to obtain high-density (> 98%) polycrystalline samples with different grain sizes. Samples with a grain size of 0.42 μm, 42 μm, and 110 μm were obtained by sintering at 1220 °C for 8 h, 1350 °C for 2 h, and 1350 °C for 8 h, respectively. More details about the microstructure of the obtained samples are given in Supporting Information S1. The sintered specimens were cut into 5 mm x 5 mm x 1.5 mm samples using a cutting machine (IsoMet Low-Speed Precision Cutter, Buehler). The surfaces of the cut samples were carefully polished in two steps to obtain samples of different thicknesses with mirror finish parallel surfaces. The final samples were heat-treated at a temperature above the Curie temperature and then were slow cooling in order to remove the internal stress generated by the cutting and polishing processes. Finally, the samples were cleaned with ethanol and acetone before their characterization.

2.2. Domains structure characterization

A Witec alpha-300RA Confocal Raman Microscope (CRM) was used to determine the ferroelectric domain configuration of each sample. Domain imaging on the surface was performed on sample regions of 10 × 10 μm for the fine-grained sample (0.42 μm of grain size). The Raman image was built from 100 × 100 spectra. For the coarse-grained samples (42 μm and 110 μm of grain size), the analyzed regions on the surface were 70 × 70 μm and 150 × 150 μm, respectively. In these cases, the Raman images were generated by surface scans of 140 × 140 and 300 × 300 spectra, respectively. A fixed acquisition time of 0.1 s per spectra was used in all cases. Topographic characterization was mapped using the AFM coupled to the CRM, operating in non-contact mode with a resonant frequency of 268 kHz, in ambient atmosphere and at room temperature. The gold-coated silicon AFM tip used in this study has 14–16 microns high, aspect ratio from 3:1 to 5:1, and a tip radius of 10 nm. Under these conditions, AFM images were captured by scanning 256 lines with 1024 points per line at 1 Hz for each sample. All the collected data were analyzed by using Witec Control Plus Software. The domain configuration is then indirectly resolved by a suitable combination of AFM and CRM imaging that shows in-plane, a, and out-of-plane, c, domains with a head-to-head configuration, thereby evidencing the occurrence of a-c-CDWs, as illustrated in Supporting Information S2. A more detailed explanation of the underlying mechanism contributing to the organization of polarization vectors can be found elsewhere [11]. Although direct measurement of CDWs is not performed here, the CDW occurrence in BTO is also supported by previous works [23–25].

2.3. Photoinduced strain measurements

A homemade optical system was designed to characterize the light-induced photo-strain. The built system allows the illumination of the samples by a diode laser (Thorlabs, Inc.) operating at a wavelength of 532 nm. The light power was controlled *via* a linear variable ND filter and was calibrated by a S121C silicon photodiode detector (Thorlabs, Inc.), ranging from 0 (dark condition) to 90 mW (maximum power of the light source). The measured elongation induced by the corresponding off-on-off illumination cycle was mapped in the regions previously studied by CRM and AFM under dark conditions. The measurement starts with the AFM mapping one-third of the total region under dark conditions. Once the first third is completed, the iris of the optical system is opened, and the second third is recorded under illumination conditions. Finally, after the second third is finished, the iris is closed, and the last third of the image is recorded under dark conditions. The off-on-off illumination sequence allows obtaining *in-situ* three regions on a single AFM image for each selected light power. Each AFM image (10 μm x 10 μm, 35 μm x 35 μm, and 75 μm x 75 μm for 0.42 μm, 42 μm and 110 μm of grain-sized samples, respectively) is obtained by scanning 256 horizontal lines at a frequency of 1 Hz. During the experiments, the samples were *in-situ* monitored by a thermal camera (FLIR Systems T440) to ensure that the thermal effect played a minor role in the photoinduced strain, as has been widely discussed elsewhere.

2.4. Optical measurements

Reflectance and transmittance measurements were performed using an integrating sphere under a single beam mode configuration, while the absorbance was calculated from the measured reflectance and transmittance values. The sample was illuminated using the same laser light source, i.e., a 532 nm laser diode (Thorlabs, Inc.), employed for the photoinduced strain measurements. The integrating sphere, RT-060-SF model (Labsphere, Inc.), was composed of two joined hemispheres coated with a highly diffuse reflective coating over the 300–2400 nm spectral range. More details about the optical setup and measurement configurations are given in Supporting Information S3.

3. Results and discussion

3.1. Photoinduced strain

Controlling mechanical strain in polycrystalline ferroelectrics by visible light was recently evidenced [16,17]. A large photo-strain, comparable to the conventional electro-strain values, was found to be related to the formation of charged domain walls (CDWs) in BTO polycrystals [17]. Two extreme cases of ferroelectric domain configuration were designed through grain size control, making it possible to show that CDWs are the functional interfaces for the light-driven domains rearrangement. Although important findings related to light control of strain in ferroelectric polycrystals were already reported, some issues remained unanswered. Fig. 1 shows a more general sight of the previous results. Grain size dependence of light-induced strain in polycrystalline BTO is shown in Fig. 1m, ranging two orders of grain size magnitude. As may be observed, fine-grained samples do not display photo-deformation (Fig. 1j), ascribed to the absence of ferroelastic CDWs, as shown in Fig. 1d, where the CRM image shows grains with a single direction of polarization. Otherwise, coarse-grained samples exhibit remarkable reversible photo-deformation (Fig. 1k and l), which is related to the appearance of CDWs, as shown in Fig. 1e and f. However, no direct correlation between light-induced strain and grain size is observed, suggesting the strain does not continue to increase once a similar domain structure is stabilized.

A quasi-linear dependence between the photo-strain and light power density is verified for coarse-grained samples (Supporting Information S4). Nonetheless, instead of grain size, another sample feature seems to

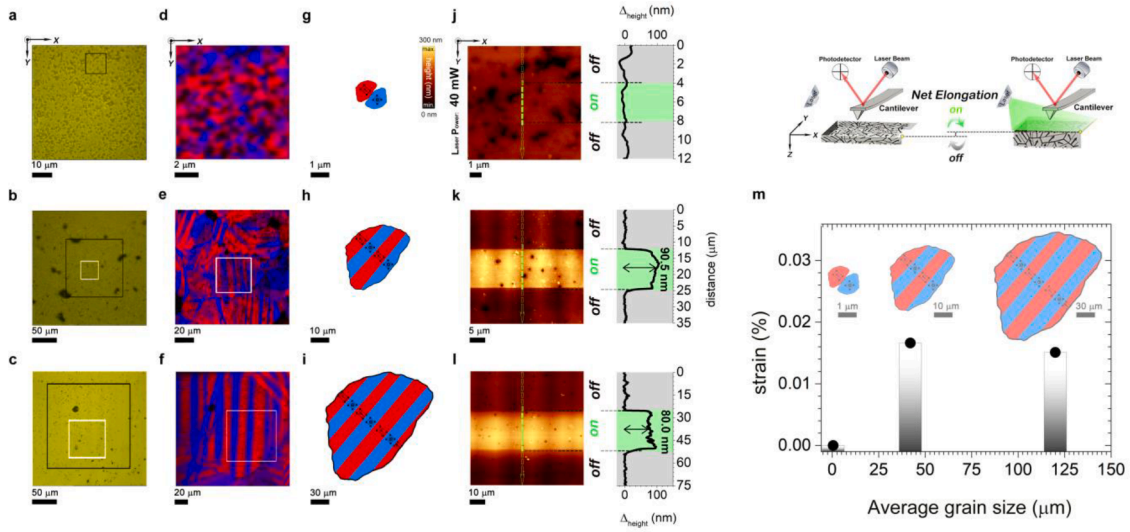

Fig. 1. Grain size effect on the light-induced strain in polycrystalline BTO. (a–c) Optical images of the surface of BTO samples with a grain size of (a) 0.42 μm, (b) 42 μm, and (c) 110 μm. Black squares in (a–c) show the regions where the surface confocal Raman images (d–f) are taken for each sample. White squares in panels (b,c) indicate the regions where the topographic images (k,l) are acquired by AFM for coarse-grained samples, while all regions of panel (d) is mapped to obtain the AFM image (j) for fine-grained sample. (g–i) Schematic representation of domain structure for each sample. The same light power of 40 mW is used to obtain the set of AFM images (j–l), revealing a reversible light-induced elongation for coarse-grained samples. The topography profile along the dashed arrows in (j–l) is plotted right to each AFM image. (m) Bar graph summarizing the light-induced strain for all samples at 40 mW of light power. All samples have the same thickness of ~530 μm. Additionally, a simplified experimental scheme for measuring light-induced strain is shown above the panel (m).

be the key factor for attaining the major photo response because no larger photo strain is achieved for the sample with larger grain size. The domain structure of coarse-grained samples is mainly composed of a sequence of twinned head-to-head and tail-to-tail 90°-domains leading to the formation of CDWs. It is well known that domain wall density depends on grain size [26,27]; as is shown in Fig. 1d–f, being CDW density higher for BTO with medium grain size (42 μm) than for BTO with large grain size (110 μm). This experimental evidence is irrefutable proof that CDWs are the functional interfaces for the light-induced strain in BTO.

Once a direct correlation between light-induced strain and domain structure seems to be established, other sample features should be considered to shed more light on this light-matter coupling phenomenon in ferroelectric polycrystals. In this respect, large grain-sized samples with different thicknesses are photo-stimulated in order to show how the sample thickness modulates both the absolute and relative values of the photoinduced elongation (Fig. 2). Fig. 2g–i illustrate the thickness dependence of absolute photoinduced elongation. As may be observed, the elongation boosts as sample thickness increases, whereas the photo-strain decreases (Fig. 2j). Assuming samples have the same CDWs density, these results can be explained as a consequence of the light attenuation. Light intensity drops dramatically (ideally exponentially) when

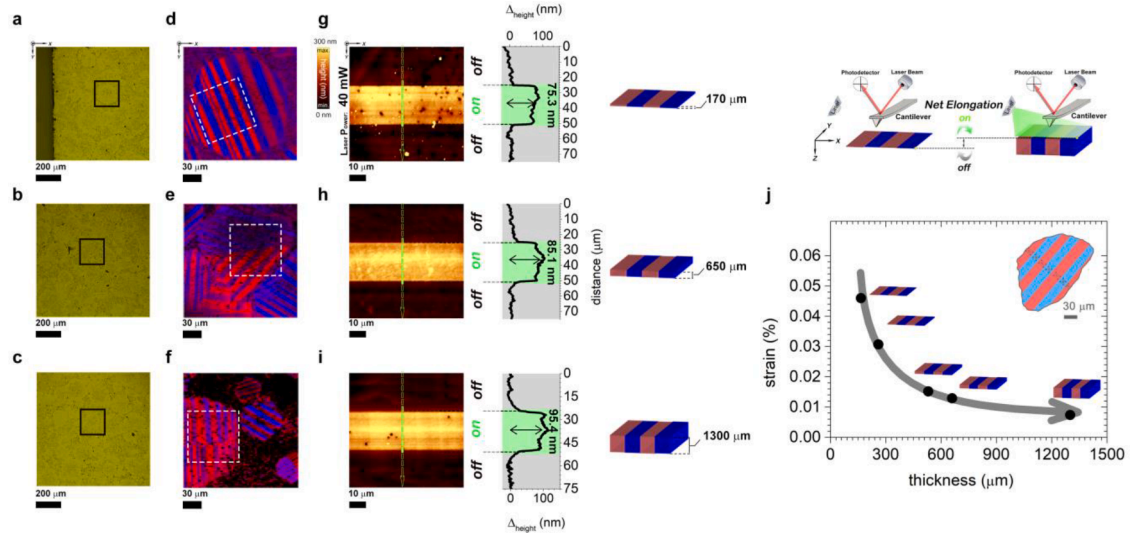

Fig. 2. Light-induced strain of the sample thickness in polycrystalline BTO. (a–c) Optical images of the surface of 110 μm grain-sized BTO samples with a thickness of ~170 μm (a), ~650 μm (b), and ~1300 μm (c). Black squares in (a–c) show the regions where the surface confocal Raman images (d–f) are taken for each sample. White squares in (d–f) indicate the regions where the topography AFM images are acquired. (g–i) AFM images revealing a reversible light-induced elongation for all samples. (j) Thickness dependence of the light-induced strain for 110 μm grain-sized BTO. The same light power of 40 mW is applied to all samples. Additionally, a simplified experimental scheme for measuring light-induced strain is shown above the panel (j). The dark spots revealed in topographic images are residual porosity from the sintering process, which is a common feature of ceramic materials.

penetrating the material, such that more CDWs interact with light as the thickness increases but in a weaker fashion. Therefore, elongation increases while strain decreases as the sample thickness rises.

3.2. Optical absorption and band gap

According to the above results, light absorption at CDWs seems to determine the photo response. In order to deepen this assertion, the absorption coefficient is calculated from the optical absorbance values for all samples. Results are shown in Fig. 3 as a function of the sample grain size (Fig. 3a) as well as the sample thickness (Fig. 3b). Grain boundaries are well-known to be light-absorbing interfaces such that lower absorbance would be expected as grain size increases. Obviously, this would be factual whether grain boundaries were the only contribution to the light absorption, but CDWs in BTO play a relevant role as light-absorbing entities. As shown in Fig. 3a, the absorption coefficient does not follow a well-defined trend as grain size increases. The light absorption in the fine-grained sample can be ascribed only to grain boundaries since no CDWs are formed in this sample (Fig. 1d). Contrary to what is expected from grain boundaries contribution, the light absorption is greater in the coarse-grained sample with medium grain size than in fine-grained sample, which can be explained by the large contribution of CDWs to the total sample absorption. On the other hand, the sample with a larger grain size displays lower light absorption (Fig. 3a). In this case, although the absorbance comes from both grain boundaries and CDWs, these contributions are lower in the larger grain size sample than in the medium grain size sample. Regarding the sample thickness effect, Fig. 3b shows that the absorption coefficient decreases as sample thickness rises, following the same behavior as that of the strain. Moreover, it is important to point out that absorbance increases with the sample thickness in accordance with the trend followed by the absolute light-induced deformation (Supporting Information S5).

In order to reveal the influence of interfaces (i.e., grain boundaries and domain walls) on the band gap, the absorption spectrum is measured in all samples (Supporting Information S6). The band gap undergoes a clear reduction of ca. 14% (2.76 eV), 12% (2.80 eV), and 4% (3.06 eV), compared to the BTO theoretical band gap (3.2 eV), for 0.42 μm, 42 μm, and 110 μm of grain-sized samples, respectively. Results show a lower band gap as grain size decreases, as expected in $BaTiO_3$-based materials with micron-scale grain size [28]. Additionally, the presence of CDWs has been found to significantly reduce the band gap because CDWs act as segregated channels for the motion of charge carriers such that electrons diffuse to head-to-head CDWs while holes move to tail-to-tail CDWs [29,30]. Then, electrons and holes are likely to move separately along different CDWs under the internal field modified by external excitation (light in the present case), reducing the recombination rate. Although the band gap turns out to be lower than 3.2 eV in the studied samples, the used photon energy (2.3 eV) is still low enough to discard the bulk photovoltaic effect.

4. Discussion

Based on our observations, a clear interrelationship exists between optical absorption and photo-strain *via* light absorption at CDWs. The light absorption at CDWs with energy photons lower than the material band gap has been recently explained, taking into account the photo-induced electronic reconstruction (PER) mechanism [31], which was proposed for explaining the light absorption for radiation energies below the band gap in $LaAlO_3/SrTiO_3$ (LAO/STO) heterostructures [32, 33]. The LAO/STO is electrically very similar to CDW arrays since both systems have charged interfaces, free carriers around those interfaces, and internal electric fields arising from the charged (uncompensated) interfaces.

Although demonstrating the appearance of optical transitions in CDWs requires the full calculation of the band structure (which is beyond the scope of this work), a parallelism between the band structure of STO/LAO interfaces and CDWs can undoubtedly be established [25, 34]. For STO/LAO, the photoexcited electrons generated by the optical absorption are transferred from the valence band states of LAO-layer (the polar layer) to the conduction band states in the quantum well localized in the STO/LAO-interface. Since photon absorption creates the same amount of holes and electrons (that is, an ambipolar process), the holes created in the polar layer drift under the action of the internal electric field, which spreads from the interface to the surface LAO-layer. In the case of charged domain walls, the interface is the wall itself, and thus, the domains surrounding the wall are equivalent to the LAO-polar layer. Consequently, the photoexcited electrons are promoted from the valence band states in the domains to conduction band states in the quantum well localized in the head-to-head CDW. Furthermore, the holes are drifting towards the tail-to-tail walls by the partial depolarization field, which is spread from the head-to-head to the tail-to-tail walls.

Because of the asymmetric nature of a CDW array, the depolarization field reduction between adjacent domains results to be dissimilar and, consequently, one domain becomes more energetically favorable than the other, leading to the growth of one domain at the expense of the

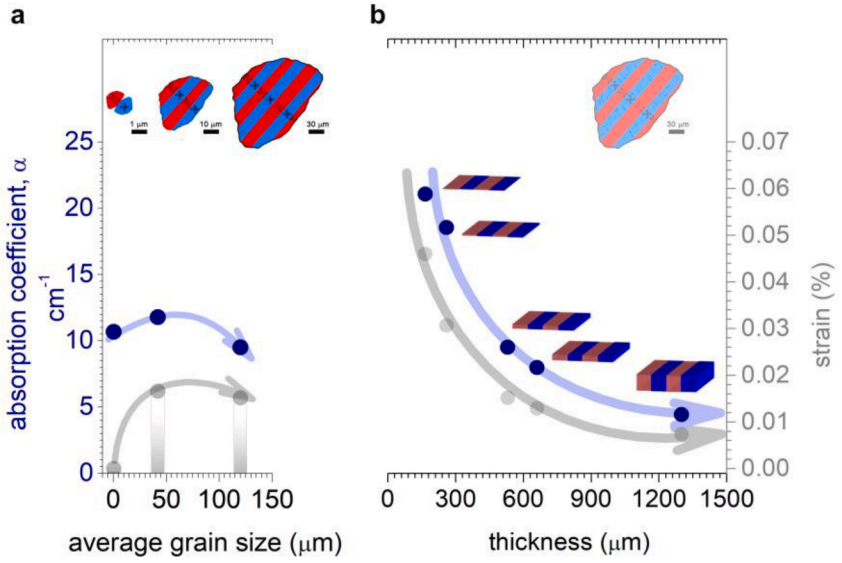

Fig. 3. Grain size and the sample thickness dependence of optical absorption in polycrystalline BTO. (a) Absorption coefficient of ~530 μm thickness polycrystalline BTO with different grain sizes. (b) Absorption coefficient of 110 μm grain-sized polycrystalline BTO with different thicknesses. The grain size and the sample thickness dependence of strain are also plotted to show a clear correlation between optical absorption and photoinduced strain. A light power of 40 mW was used for all experiments.

other, triggering the motion of the domain wall [31]. In other words, visible light changes CDW compensation such that the depolarization field modifies, fostering the domain wall motion. Therefore, a rearrangement of the domain structure occurs, and due to the ferroelastic character of the 90°-domain walls, a macroscopic net elongation is engendered. It is worth noting that the domain reconfiguration is reversible since it is a small perturbation of the ground state (dark state). Hence, light-induced strain emerges as a reversible phenomenon.

5. Conclusion

In summary, it is demonstrated that a clear interrelationship between optical absorption and light-induced strain in polycrystalline BTO there exists. The photo-response is unswervingly linked to light absorption at CDWs since no photo-response is displayed when CDWs are not formed. The photoinduced electronic reconstruction phenomenon is proposed as the physical mechanism for optical absorption in CDWs. It is important to remark that the photoinduced strain enhances as sample thickness decreases, suggesting that the observed phenomenon can be more important in thick films instead of bulk materials, thereby opening a feasible way to achieve a new generation of micro-scale photo-controlled ferroelectric-based devices. Future efforts on photo-controlled nanoactuators should be conducted toward designing more complex device architectures based on thickness gradients that could be built to obtain photo-controlled nanoactuators with wide functionalities.

CRediT authorship contribution statement

Fernando Rubio-Marcos: Conceptualization, Methodology, Visualization, Supervision, Writing – original draft, Project administration, Funding acquisition, Writing – review & editing. **Paula Pamies:** Methodology, Investigation, Validation, Formal analysis. **Adolfo Del Campo:** Methodology, Investigation. **Jordi Tiana:** Methodology, Formal analysis, Writing – review & editing. **Jonathan Ordoñez-Pimentel:** Validation, Investigation, Resources. **Michel Venet:** Methodology, Resources, Project administration. **Rocío E. Rojas-Hernandez:** Investigation. **Diego A. Ochoa:** Validation. **José F. Fernández:** Project administration, Funding acquisition. **José E. García:** Conceptualization, Methodology, Visualization, Supervision, Writing – original draft, Project administration, Funding acquisition, Writing – review & editing.

Declaration of Competing Interest

The authors declare that they have no known competing financial interests or personal relationships that could have appeared to influence the work reported in this paper.

Data availability

Data will be made available on request.

Acknowledgments

This work is supported by the AEI (Spanish Government) projects PGC2018-099158-B-I00 and PID2020-114192RB-C41. M.V. acknowledges support from the São Paulo Research Foundation FAPESP (grant number 2022/08030-5) and the Brazilian CNPq (process 304144/2021-5). J.E.G. wishes to thank the Becas Iberoamérica Santander Investigación 2020–2021 program for their financial support. F.R-M. is indebted to Comunidad de Madrid for the financial support through the Doctorados Industriales project (IND2020/IND-17375), which is co-financed by the European Social Fund.

Supplementary materials

Supplementary material associated with this article can be found, in the online version, at doi:10.1016/j.apmt.2023.101838.

References

[1] P. Poosanaas, K. Tonooka, K. Uchino, Photostrictive actuators, Mechatronics 10 (2000) 467, https://doi.org/10.1016/S0957-4158(99)00073-2.
[2] B. Kundys, Photostrictive materials, Appl. Phys. Rev. 2 (2015), 011301, https://doi.org/10.1063/1.4905505.
[3] C. Chen, Z. Yi, Photostrictive effect: characterization techniques, materials, and applications, Adv. Funct. Mater. 31 (2021), 2010706, https://doi.org/10.1002/adfm.202010706.
[4] N.I. Zheludev, E. Plum, Reconfigurable nanomechanical photonic metamaterials, Nat. Nanotechnol. 11 (2016) 16–22.
[5] L. Midolo, A. Schliesser, A. Fiore, Nano-opto-electro-mechanical systems, Nat. Nanotechnol. 13 (2018) 11, https://doi.org/10.1038/s41565-017-0039-1.
[6] C. Chen, X. Li, T. Lu, Y. Liu, Z. Yi, Reinvestigation of the photostrictive effect in lanthanum-modified lead zirconate titanate ferroelectrics, J. Am. Ceram. Soc. 103 (2020) 4074, https://doi.org/10.1111/jace.17172.
[7] Y. Bai, Photoresponsive piezoelectrics, Front. Mater. 8 (2021), 636712, https://doi.org/10.3389/fmats.2021.636712.
[8] S. Matzen, L. Guillemot, T. Maroutian, S.K.K. Patel, H. Wen, A.D. DiChiara, G. Agnus, O.G. Shpyrko, E.E. Fullerton, D. Ravelosona, P. Lecoeur, R. Kukreja, Tuning ultrafast photoinduced strain in ferroelectric-based devices, Adv. Electron. Mater. 5 (2019), 1800709, https://doi.org/10.1002/aelm.201800709.
[9] B. Kundys, M. Viret, D. Colson, D.O. Kundys, Light-induced size changes in $BiFeO_3$ crystals, Nat. Mater. 9 (2010) 803, https://doi.org/10.1038/nmat2807.
[10] C. Paillard, S. Prosandeev, L. Bellaiche, *Ab initio* approach to photostriction in classical ferroelectric materials, Phys. Rev. B 96 (2017), 045205, https://doi.org/10.1103/PhysRevB.96.045205.
[11] F. Rubio-Marcos, A. Del Campo, P. Marchet, J.F. Fernández, Ferroelectric domain wall motion induced by polarized light, Nat. Commun. 6 (2015) 6594, https://doi.org/10.1038/ncomms7594.
[12] F. Rubio-Marcos, D.A. Ochoa, A. Del Campo, M.A. García, G.R. Castro, J. F. Fernández, J.E. García, Reversible optical control of macroscopic polarization in ferroelectrics, Nat. Photon. 12 (2018) 29, https://doi.org/10.1038/s41566-017-0068-1.
[13] F. Rubio-Marcos, D. Páez-Margarit, D.A. Ochoa, A. Del Campo, J.F. Fernández, J. E. García, Photo-controlled ferroelectric-based nanoactuators, ACS Appl. Mater. Interfaces 11 (2019) 13921, https://doi.org/10.1021/acsami.9b01628.
[14] B. Narayan, J.S. Malhotra, R. Pandey, K. Yaddanapudi, P. Nukala, B. Dkhil, A. Senyshyn, R. Ranjan, Electrostrain in excess of 1% in polycrystalline piezoelectrics, Nat. Mater. 17 (2018) 427–431, https://doi.org/10.1038/s41563-018-0060-2.
[15] G. Vats, Y. Bai, D. Zhang, J. Juuti, J. Seidel, Optical control of ferroelectric domains: nanoscale insight into macroscopic observations, Adv. Opt. Mater. 7 (2019), 1800858, https://doi.org/10.1002/adom.201800858.
[16] X. Li, C. Chen, F. Zhang, X. Huang, Z. Yi, Large visible-light-driven photostriction in $Bi(Ni_{2/3}Nb_{1/3})O_3$–$PbTiO_3$ ferroelectrics, APL Mater. 8 (2020), 061111, https://doi.org/10.1063/5.0010011.
[17] F. Rubio-Marcos, A. Del Campo, J. Ordoñez-Pimentel, M. Venet, R.E. Rojas-Hernandez, D. Páez-Margarit, D.A. Ochoa, J.F. Fernández, J.E. García, Photocontrolled strain in polycrystalline ferroelectrics *via* domain engineering strategy, ACS Appl. Mater. Interfaces 13 (2021) 20858, https://doi.org/10.1021/acsami.1c03162.
[18] G. Vats, Y. Bai, J. Seidel, Optomechanical mapping of ferroelectric domains and the piezo-photovoltaic effect in Ba- and Ni-doped $(K_{0.5}Na_{0.5})NbO_3$, Adv. Photonics Res. 2 (2021), 2100050, https://doi.org/10.1002/adpr.202100050.
[19] F. Rubio-Marcos, A. Del Campo, R.E. Rojas-Hernandez, M.O. Ramírez, R. Parra, R. U. Ichikawa, L.A. Ramajo, L.E. Bausá, J.F. Fernández, Experimental evidence of charged domain walls in lead-free ferroelectric ceramics: light-driven nanodomain switching, Nanoscale 10 (2018) 705–715, https://doi.org/10.1039/C7NR04304J.
[20] P.S. Bednyakov, B.I. Sturman, T. Sluka, A.K. Tagantsev, P.V. Yudin, Physics and applications of charged domain walls, NPJ Comput. Mater. 4 (2018) 65, https://doi.org/10.1038/s41524-018-0121-8.
[21] J. Seidel, Nanoelectronics based on topological structures, Nat. Mater. 18 (2019) 188–190, https://doi.org/10.1038/s41563-019-0301-z.
[22] P. Sharma, P. Schoenherr, J. Seidel, Functional ferroic domain walls for nanoelectronics, Materials (Basel) 12 (2019) 2927, https://doi.org/10.3390/ma12182927.
[23] M.Y. Gureev, A.K. Tagantsev, N. Setter, Head-to-head and tail-to-tail 180° domain walls in an isolated ferroelectric, Phys. Rev. B 83 (2011), 184104, https://doi.org/10.1103/PhysRevB.83.184104.
[24] T. Sluka, A.K. Tagantsev, D. Damjanovic, M.Y. Gureev, N. Setter, Enhanced electromechanical response of ferroelectrics due to charged domain walls, Nat. Commun. 3 (2012) 748, https://doi.org/10.1038/ncomms1751.
[25] T. Sluka, A.K. Tagantsev, P. Bednyakov, N. Setter, Free-electron gas at charged domain walls in insulating $BaTiO_3$, Nat. Commun. 4 (2013) 1808, https://doi.org/10.1038/ncomms2839.
[26] G. Arlt, Twinning in ferroelectric and ferroelastic ceramics: stress relief, J. Mater. Sci. 25 (1990) 2655–2666, https://doi.org/10.1007/BF00584864.

[27] M. Frey, D. Payne, Grain-size effect on structure and phase transformations for barium titanate, Phys. Rev. B 54 (1996) 3158–3168, https://doi.org/10.1103/PhysRevB.54.3158.
[28] H. Qi, A. Xie, A. Tian, R. Zuo, Superior energy-storage capacitors with simultaneously giant energy density and efficiency using nanodomain engineered $BiFeO_3$-$BaTiO_3$-$NaNbO_3$ lead-free bulk ferroelectrics, Adv. Energy Mater. 10 (2020), 1903338, https://doi.org/10.1002/aenm.201903338.
[29] J. Seidel, D. Fu, S.Y. Yang, E. Alarcón-Lladó, J. Wu, R. Ramesh, J.W. Ager, Efficient photovoltaic current generation at ferroelectric domain walls, Phys. Rev. Lett. 107 (2011), 126805, https://doi.org/10.1103/PhysRevLett.107.126805.
[30] S. Liu, F. Zheng, N.Z. Koocher, H. Takenaka, F. Wang, A.M. Rappe, Ferroelectric domain wall induced band gap reduction and charge separation in organometal halide perovskites, J. Phys. Chem. Lett. 6 (2015) 693–699, https://doi.org/10.1021/jz502666j.
[31] J. Ordoñez-Pimentel, M. Venet, D.A. Ochoa, F. Rubio-Marcos, J.F. Fernández, J. E. García, Light-driven motion of charged domain walls in isolated ferroelectrics, Phys. Rev. B 106 (2022), 224110, https://doi.org/10.1103/PhysRevB.106.224110.
[32] E. Di Gennaro, U.S. di Uccio, C. Aruta, C. Cantoni, A. Gadaleta, A.R. Lupini, D. Maccariello, D. Marré, I. Pallecchi, D. Paparo, P. Perna, M. Riaz, F.M. Granozio, Persistent photoconductivity in 2D electron gases at different oxide interfaces, Adv. Opt. Mater. 1 (2013) 834, https://doi.org/10.1002/adom.201300150.
[33] E. Di Gennaro, U. Coscia, G. Ambrosone, A. Khare, F.M. Granozio, U.S. di Uccio, Photoresponse dynamics in amorphous-$LaAlO_3$/$SrTiO_3$ interfaces, Sci. Rep. 5 (2015) 8393, https://doi.org/10.1038/srep08393.
[34] X. Wu, D. Vanderbilt, Theory of hypothetical ferroelectric superlattices incorporating head-to-head and tail-to-tail 180° domain walls, Phys. Rev. B 73 (2006), 020103, https://doi.org/10.1103/PhysRevB.73.020103.